American Mineralogist, Volume 97, pages 707–712, 2012

Crystal structure and thermal expansion of aragonite-group carbonates by single-crystal X-ray diffraction

Yu Ye,[1,*] Joseph R. Smyth,[2] and Paul Boni[2]

[1]Department of Physics, University of Colorado, Boulder, Colorado 80309, U.S.A.
[2]Department of Geological Sciences, University of Colorado, Boulder, Colorado 80309, U.S.A.

Abstract

Crystal structures of four aragonite-group carbonates—aragonite ($Ca_{0.997}Sr_{0.003}CO_3$), calcian strontianite ($Ca_{0.147}Sr_{0.853}CO_3$), cerussite ($Ca_{0.001}Pb_{0.999}CO_3$), and witherite ($Sr_{0.019}Ba_{0.981}CO_3$)—have been refined at ambient conditions, and thermal expansion has been measured over a range of temperatures from 143 to 586 K by single-crystal X-ray diffraction. Average linear thermal expansion coefficients $\alpha_0(V)$ are 58(2), 58.3(7), 64(2), and 57(2) ($\times 10^{-6}$ K^{-1}) for aragonite, strontianite, cerussite, and witherite, respectively, throughout the experimental temperature range. Aragonite, strontianite, and witherite have very similar $\alpha_0(V)$ values, whereas that of cerussite is significant larger, primarily due to the *c*-axis thermal expansion for cerussite being much larger than those of the other carbonates. There are no significant differences for $\alpha_0(a)$ values among the four carbonates, whereas $\alpha_0(b)$ values decrease in the order of aragonite > strontianite > cerussite ≈ witherite, and $\alpha_0(c)$ values increase in the order of aragonite < strontianite < witherite < cerussite. Crystal structures were refined for aragonite (184 to 527 K). <Ca-O> vs. *T* (K) is fitted linearly quite well, with a slope of $5.8(8) \times 10^{-6}$ (Å/K). Corrected for assumed rigid body motion, the CO_3 groups showed no significant change in C-O distances over the temperature range.

Keywords: Aragonite, strontianite, cerussite, witherite, thermal expansion, crystal structure

Introduction

Aragonite ($CaCO_3$), the most common orthorhombic carbonate, crystallizes in space group *Pmcn*, and consists of layers of 9-coordinated Ca^{2+} cations in approximate hexagonal closest packing, alternating with layers of planar CO_3 groups stacked perpendicular to the *c*-axis, (Bragg 1924; Wyckoff 1925). Although orthorhombic, the structure approaches trigonal symmetry, and crystals commonly show pseudo-hexagonal morphology. Strontianite ($SrCO_3$), cerussite ($PbCO_3$), and witherite ($BaCO_3$) also have the aragonite structure, and as the M^{2+} cation (Ca^{2+} < Sr^{2+} < Pb^{2+} < Ba^{2+}) size increases, the trigonal crystal structure becomes less and less distorted so that the structure of witherite is closest to ideal (Speer 1983). Recent studies of aragonite-group structures have been carried out at various temperature and pressure conditions (Pannhorst and Löhn 1970; De Villiers 1971; Dal Negro and Ungaretti 1971; Dickens and Bowen 1971; Jarosch and Heger 1986, 1988; Chevrier et al. 1992, Pilati et al. 1998; Holl et al. 2000; Bevan et al. 2002; Caspi et al. 2005; Pokroy et al. 2007; Antao and Hassan 2009).

High-temperature studies of phase transformations in carbonates of the aragonite group have been reported by Lander (1949), Baker (1962), Weinbruch et al. (1992), Lin and Liu (1996 and 1997), and Antao and Hassan (2007, 2010). In the current study, the unit-cell parameters for aragonite, strontianite, cerussite, and witherite are measured at low and high temperatures to investigate the effect of M^{2+} cation size on the volume and anisotropy of thermal expansion, by single-crystal diffraction. Since the single crystals break down at high temperatures before any phase change occurs, no phase transformation was observed in this study. Results for thermal expansion are compared with coherent compressibility studies by Martinez et al. (1996), Holl et al. (2000), and Liu et al. (2005). In addition, atom positions of aragonite have been refined from single-crystal intensity measurements collected at low and high temperatures to investigate its crystal structure dependence on temperature.

Experimental methods and results

The carbonate group samples for the current study are all from natural sources. The aragonite was a purchased specimen, no locality was available. The calcian strontianite (CU collection Number 4270) is from Dreisteinfurt, Westphalia, Germany; the cerussite (CU collection Number 4552) is from Tsumeb, Namibia; and the witherite (CU collection Number 5914) is from Hexham, Northumberland, England (Holl et al. 2000). A single crystal about 300–400 μm for each sample was selected for chemical analysis by electron microprobe. Each sample was mounted in epoxy and polished on the surface. Mineral compositions were determined using a JEOL 8600 SuperProbe, operating at a 15 kV accelerating voltage and 20 nA beam current, with a 5 μm beam size to reduce volatility of CO_2. Certified mineral standards were used (galena for Pb, barite for Ba, wollastonite for Ca, strontianite for Sr, olivine for Mg, and garnet for Fe and Mn) for quantification using ZAF wavelength-dispersive corrections. On each sample, ~6–7 points were chosen for measuring the weight percentages of oxides, and the average values with standard deviations are listed in Table 1. The formulas of the carbonate samples are summarized as: aragonite $Ca_{0.997}Sr_{0.003}CO_3$; calcian strontianite $Ca_{0.147}Sr_{0.853}CO_3$; cerussite $Ca_{0.001}Pb_{0.999}CO_3$; witherite $Sr_{0.019}Ba_{0.981}CO_3$.

Crystals of aragonite (120 × 76 × 70 μm), calcian strontianite (110 × 100 × 84 μm), cerussite (105 × 75 × 68 μm), and witherite (153 × 90 × 62 μm), without visible inclusions or defects, were chosen for the refinements of unit-cell parameters and crystal structures at ambient conditions. Measurements for unit-cell refinements were conducted on a Bruker P4 four-circle diffractometer with a dual scintillation

* E-mail: yey@colorado.edu

0003-004X/12/0004–707$05.00/DOI: http://dx.doi.org/10.2138/am.2012.3923

TABLE 1. Results of electron-microprobe analyses

	Aragonite	Strontianite	Cerussite	Witherite
CaO (wt%)	55.5(5)	5.9(4)	0.03(1)	0.01(1)
SrO	0.26(4)	62.5(8)	0.05(2)	0.98(5)
MgO	0.00(1)	0.01(1)	0	0
FeO	0.02(2)	0.01(1)	0.01(2)	0.02(3)
BaO	0.01(1)	0.02(2)	0.01(1)	76.7(2)
PbO	0.01(2)	0.01(2)	83.4(5)	0.01(1)
MnO	0	0.01(1)	0.01(1)	0
CO_2*	43.7(5)	31.1(9)	16.5(5)	22.4(3)
Total	99.5(5)	99.6(8)	100.0(5)	100.3(5)
Ca (apfu)	0.997(9)	0.147(3)	0.001	0.000
Sr	0.003(1)	0.853(8)	0.000	0.019(1)
Mg	0.000	0.000	0.000	0.000
Fe	0.000	0.000	0.000	0.000
Ba	0.000	0.000	0.000	0.989(3)
Pb	0.000	0.000	0.999(6)	0.000
Mn	0.000	0.000	0.000	0.000
CO_3*	1.000(11)	1.00(2)	1.00(3)	1.000(7)

* Calculated from stoichiometry, assuming the ratio of C:O to be 1:3.

point-detector system using an 18 kW rotating Mo-anode X-ray generator, which was operated at 50 kV and 250 mA. The X-ray has two characteristic wavelengths ($K\alpha_1$ = 0.709300 Å and $K\alpha_2$ = 0.713590 Å), and a single crystal of anhydrous forsterite with spherical shape was used to calibrate $K\alpha_{\_average}$ = 0.71065 Å, which was used for later unit-cell and crystal-structure refinements in the following discussion. Up to 48 reflections with $10° < 2\theta < 30°$ from each crystal were centered and unit-cell parameters refined by a least-squares-fitting using the software package XSCANS (Bruker 1996). Subsequently, intensity data were collected using a Bruker APEX II CCD detector mounted on a P4 diffractometer. The refined unit-cell and intensity scan parameters are listed in Table 2. The atomic position coordinates and anisotropic displacement parameters were refined using the program SHELXL-97 (Sheldrick 1997) in the software package of WinGX (Farrugia 1999), and are listed in Table 3 and Appendix 1[1], respectively. The XtalDraw software package (Downs et al. 1993) was used to calculate the bond lengths, angles, and coordination parameters listed in Table 4. CIF files also available on deposit.[1]

The refinements of cell parameters at low-temperature (below 300 K) and high-temperature ranges (above 300 K) were conducted on the point-detector system to determine axial and volumetric thermal expansion coefficients. For low-temperature measurements, each single crystal was cooled to temperatures as low as 143 K from room temperature. Low temperatures were measured and controlled by a Bruker LT-2A controller, which uses a low-temperature N_2 gas stream. For high-temperature experiments, another single crystal from the same source sample of each carbonate was mounted inside a silica glass capillary and heated from 300 to 586 K for aragonite, strontianite, and witherite, and to 489 K for cerussite because the single crystal of cerussite broke down above 489 K. Heating was accomplished using a Bruker high-temperature device, which used a two-prong ceramic-coated Pt wire radiant heater, with an Omega temperature-control unit. There were differences between the real temperatures at the crystal positions and the ones read from the devices due to the distance between the tip of the thermal couple and sample position, and temperature calibration was conducted as outlined in Ye et al. (2009). The refined unit-cell parameters vs. calibrated temperatures for both low- and high-temperature ranges of aragonite, strontianite, cerussite, and witherite are listed in Appendixes 2, 3, 4, and 5[1], respectively. Temperature uncertainties are about 2 K at low temperatures and about 5 K for high temperatures (Ye et al. 2009).

For the aragonite sample at low and high temperatures, intensity scans were conducted on the point-detector diffractometer system after measuring unit-cell parameters at each temperature point. For the low-temperature range, intensity scans were conducted at 300, 265, 224, and 184 K, but not 143 K, because at 143 K, ice condensate piled up rapidly at the tip of the gas nozzle, which affected the intensities. For high-temperature range, intensity scans were carried at 300, 359, 415, 471, and 527 K, but not 586 K, because the crystal became somewhat defective at 586 K, and the refined unit-cell parameters had much larger uncertainties than those at lower temperatures. Above 586 K, the crystal broke up, and reflections could not be effectively centered for unit-cell refinement. For each intensity scan, the 2θ scan range was set to 30°, with $-3 \le h \le 3$, $-5 \le k \le 5$, $-4 \le l \le 4$. For example, we collected the (111) unique reflection with an eightfold redundancy for the orthorhombic structure. For each intensity scan at high temperatures, more than 300 reflections were measured, of which 56 were unique, while at low temperatures, the number of total reflections for each intensity scan decreased by about 20%, and the number of unique reflections decreased to 51. During low-temperature measurement, the χ angle scan range was limited to –55°–250° due to the rotation limitation by the cooling device, and reflections with χ from 250 to 305° were omitted from the scan process. The intensity scan parameters for aragonite at temperatures are listed in Table 5, the refined atomic position coordinates and displacement parameter (U_{eq}) are listed in Appendix 6[1], and calculated bond lengths and angles are listed in Appendix 7[1]. The data processes were performed with the same software as those for ambient condition mentioned above. At high temperatures, the displacement parameters of O [U_{eq}(O1) and U_{eq}(O2)] became significantly larger than that of C [U_{eq}(C)]. CO_3 groups were treated as rigid bodies during thermal expansion, and the rigid-body correction is applied to C-O bond lengths (Downs et al. 1992; Hazen et al. 2000), as in Equation 1

$$(R_{SRB})^2 = R^2 + 3[U_{eq}(O1) - U_{eq}(C)] \quad (1)$$

where R_{SRB} is the length of the simple rigid bond, and R is the observed bond length.

DISCUSSION

Unit-cell parameters and bond lengths at room temperature

Antao and Hassan (2009) conclude that *a*, *b*, and *c* axes increase linearly as functions of unit-cell volume. The unit-cell axes vs. volumes are plotted in Figure 1, and essentially linear trends

TABLE 2. Unit-cell parameters and intensity data collection parameters at ambient condition

	Aragonite	Strontianite	Cerussite	Witherite
a (Å)	4.9596(5)	5.0914(6)	5.1820(4)	5.3193(9)
b (Å)	7.9644(7)	8.3519(8)	8.4953(9)	8.9056(8)
c (Å)	5.7416(5)	5.9901(7)	6.1436(5)	6.4353(9)
V (Å^3)	226.80(4)	254.72(5)	270.46(4)	304.85(7)
Max 2θ scanned	59.5°	48.8°	66.9°	63.1°
No. of refl.	3370	2779	6543	5206
No. unique	357	231	574	557
No. unique ($I > 2\sigma$)	300	171	375	374
R_1 for $I > 2\sigma$	0.0239	0.0469	0.0333	0.0455
GoF for all data	1.068	1.628	1.103	1.463

TABLE 3. Atomic position coordinates at ambient condition

		Aragonite	Strontianite	Cerussite	Witherite
M	*y/b*	0.41498(5)	0.4160(1)	0.41706(5)	0.41631(7)
	z/c	0.75936(7)	0.7573(2)	0.75405(6)	0.75452(7)
C	*y/b*	0.7622(3)	0.757(2)	0.765(2)	0.757(1)
	z/c	–0.0851(4)	–0.086(2)	–0.090(2)	–0.079(1)
O1	*y/b*	0.9220(2)	0.912(1)	0.913(1)	0.9011(8)
	z/c	–0.0956(3)	–0.092(2)	–0.094(2)	–0.089(1)
O2	*x/a*	0.4737(2)	0.469(1)	0.463(1)	0.4611(9)
	y/b	0.6807(1)	0.6800(7)	0.6864(8)	0.6840(6)
	z/c	–0.0872(2)	–0.085(1)	–0.087(1)	–0.0827(8)

TABLE 4. Bond lengths (Å) and bond angles

	Aragonite	Strontianite	Cerussite	Witherite
M O1 (×1)	2.417(2)	2.536(9)	2.585(6)	2.742(7)
O1 (×2)	2.653(2)	2.732(9)	2.771(6)	2.869(7)
O2 (×2)	2.450(2)	2.562(9)	2.665(6)	2.760(7)
O2 (×2)	2.517(2)	2.643(9)	2.676(6)	2.804(7)
O2 (×2)	2.547(2)	2.646(9)	2.722(6)	2.836(7)
<M-O>	2.528(2)	2.634(9)	2.695(6)	2.809(7)
C O1 (×1)	1.274(4)	1.29(2)	1.26(1)	1.28(1)
O2 (×2)	1.286(4)	1.28(2)	1.29(1)	1.30(1)
<C-O>	1.282(4)	1.29(2)	1.28(1)	1.29(1)
O1-C-O2 (×2)	120.3(3)°	120.0(9)°	121.1(7)°	120.0(8)°
O2-C-O2 (×1)	119.3(3)°	119.9(9)°	117.8(7)°	119.9(8)°
<O-C-O>	120.0(3)°	120.0(9)°	120.0(7)°	119.9(8)°

[1] Deposit item AM-12-020, CIF, Appendix Tables. Deposit items are available two ways: For a paper copy contact the Business Office of the Mineralogical Society of America (see inside front cover of recent issue) for price information. For an electronic copy visit the MSA web site at http://www.minsocam.org, go to the *American Mineralogist* Contents, find the table of contents for the specific volume/issue wanted, and then click on the deposit link there.

TABLE 5. Data-collection parameters of intensity scan for aragonite at temperatures

T (K)	184	224	265	300*	300†	359	415	471	527
No. refl.	250	247	239	246	306	304	306	306	307
No. unique	51	51	51	51	55	56	56	56	56
No. unique ($I > 4\sigma$)	50	49	49	49	50	51	52	50	52
R_1 for $I > 4\sigma$	0.0225	0.0226	0.0265	0.0228	0.0213	0.0185	0.0283	0.0175	0.0213
R_1 for all	0.0230	0.0232	0.0275	0.0231	0.0530	0.0466	0.0603	0.0518	0.0495
GoF for all	1.966	1.519	1.934	1.842	1.360	1.057	1.448	1.175	1.483

* Intensity scan data at room temperature for the crystal used for low-temperature experiments.
† Intensity scan data at room temperature for the crystal used for high-temperature measurements.

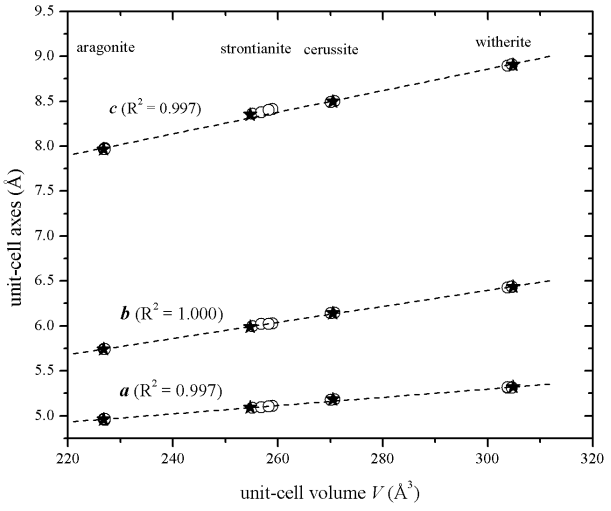

FIGURE 1. Unit-cell axes vs. volumes as linear functions. The solid five-star symbols are for current study, and open circle symbols are from Antao and Hassan (2007, 2009, 2010), Chevrier et al. (1992), De Villiers (1971), Dal Negro and Ungaretti (1971), Holl et al. (2000), Jarosch and Heger (1986, 1988), Pannhorst and Löhn (1970), and Pokroy et al. (2007). [The data for Antao and Hassan (2007, 2009) and Holl et al. (2000) are measured at ambient condition.]

are supported by the data from the current and previous studies as shown in Figure 1. The unit-cell parameters for aragonite from this and previous studies agree quite well (Antao and Hassan 2009, 2010; Dal Negro and Ungaretti 1971; De Villiers 1971; Jarosch and Heger 1986). The discrepancy of unit-cell parameters for strontianite from different studies are most significant; the cell parameters (and thus volume) decrease in the order of Antao and Hassan (2009) > Pannhorst and Löhn (1971) > De Villiers (1971) > current study. For example, the cell volume of strontianite from Antao and Hassan (2009) is about 1.6% larger than that from this study. The main differences between the current and previous measurements are likely due to the relatively higher Ca content (14.7% apfu) of our strontianite sample. The cell volume of witherite from Antao and Hassan (2007, 2009) is also about 0.3% larger than those from Holl et al. (2000) and De Villiers (1971), but are in close agreement with those of the current study. In addition, The *a*:*b*:*c* ratios from current study are 1:1.61:1.16 for aragonite; 1:1.64:1.18 for strontianite; 1:1.64:1.19 for cerussite; and 1:1.67:1.21 for witherite.

Neutron diffraction gives higher precision than X-ray diffraction for position parameters of light atoms, such as C and O. The <M-O> and <C-O> values from this study and previous studies by neutron diffractions are summarized in Table 6. The refinements of strontianite show most significant differences between this study and previous neutron diffraction studies due to higher Ca content in our strontianite sample.

TABLE 6. Comparison of unit-cell volume and average bond lengths for the current single-crystal X-ray diffraction and neutron diffraction

	V (Å^3)	<M-O> (Å)	<C-O> (Å)	
Aragonite	226.80(4)	2.528(2)	1.282(4)	This study
	226.91(3)	2.5282(5)	1.2822(4)	Jarosch and Heger (1986)
	227.039(5)	2.529(2)	1.282(1)	Pokroy et al. (2007)*
Strontianite	254.72(5)	2.634(9)	1.29(2)	This study
	258.25(4)	2.648(8)	1.285(7)	Jarosch and Heger (1988)
Cerussite	270.46(4)	2.695(6)	1.28(1)	This study
	270.08(8)	2.6921(8)	1.284(1)	Chevrier et al. (1992)
Witherite	304.85(7)	2.809(7)	1.29(1)	This study
	304.614(8)	2.8099(7)	1.2873(8)	Antao et al. (2009)

* Geological sample.

Thermal expansion at low and high temperatures

For each carbonate, separate single crystals from the same sample were measured over the low- and high-temperature ranges. The unit-cell parameters at low and high temperatures are normalized to the parameters at room temperature (300 K) of each crystal, and plotted vs. temperature in Figure 2. Accordingly, normalized unit-cell parameters are equal to one for room temperature, smaller than one for low temperatures, and greater than one for high temperatures. The temperature-induced changes are greater for c/c_0 than for a/a_0 or b/b_0 (Fig. 3). The V/V_0 and c/c_0 vs. T plots are fitted to second-order polynomial, whereas a/a_0 and b/b_0 vs. T plots are linear within error. The thermal expansion coefficient, α, is defined as

$$\alpha = 1/V\,(\partial V/\partial T)_p. \quad (2)$$

The temperature dependence of α can be expressed as a linear function of T

$$\alpha = a_1 \times T + a_0. \quad (3)$$

In the current study, $|V/V_0 - 1| << 1$, then the second-order fitting of V/V_0 can be interpreted as

$$V/V_0 = \tfrac{1}{2}\, a_1 \times T^2 + a_0 \times T + C \quad (4)$$

where C is a constant from integration.

The calculated a_1, a_0, and C for each carbonate are listed in Table 7, as well as R^2 values and temperature ranges. The a_1 value for cerussite is much larger than those for aragonite, strontianite, and witherite, meaning that cerussite expands much more significantly as temperature increases.

The average axial and volume thermal expansion coeffi-

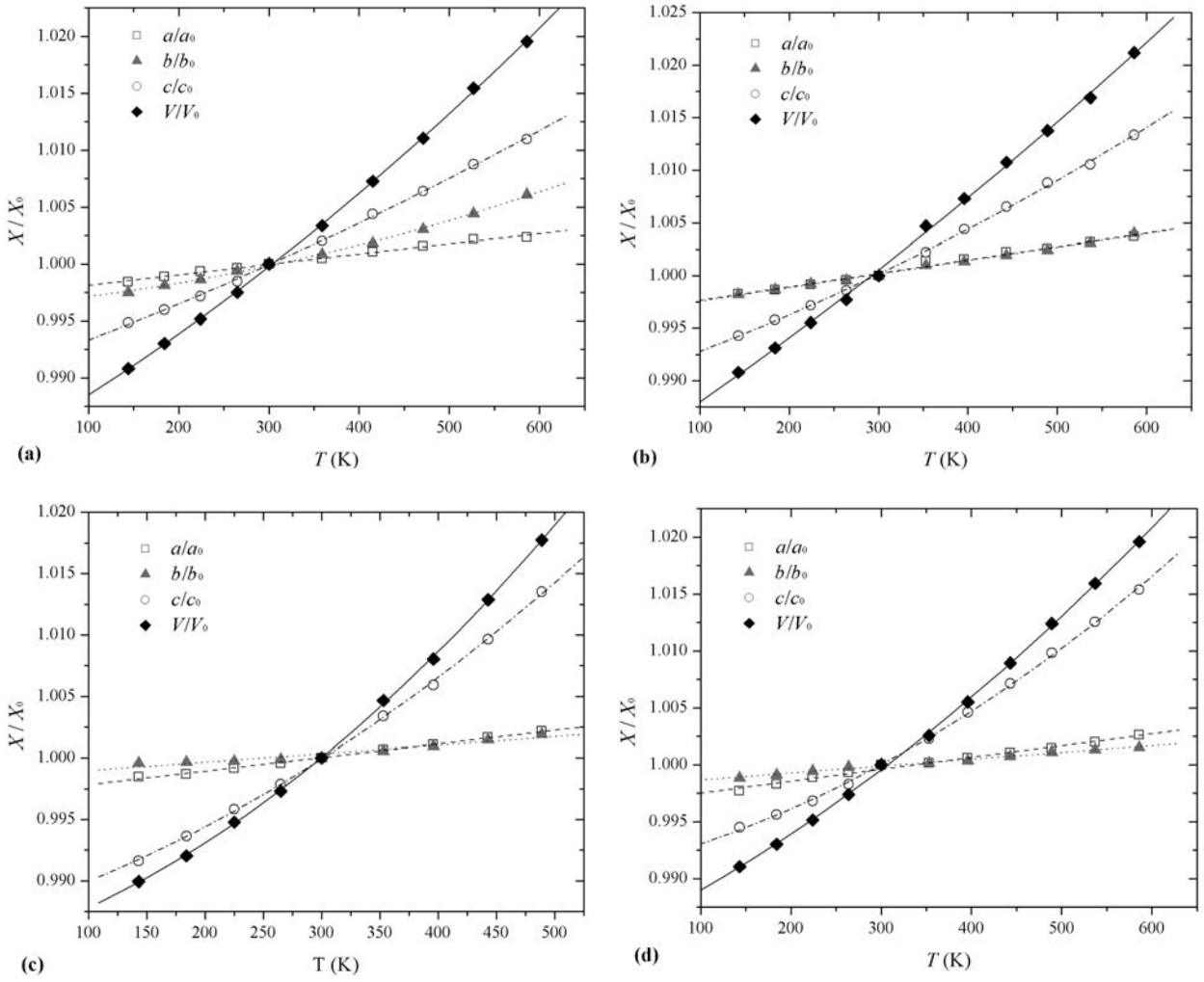

FIGURE 2. Unit-cell parameters vs. T (K), normalized to the parameters at ambient temperature for both low- and high-temperature experiments of (**a**) aragonite, (**b**) strontianite, (**c**) cerussite, and (**d**) witherite. a_0, b_0, c_0, and V_0 are the unit-cell parameters at room temperature. V/V_0 and c/c_0 vs. T are fitted to second-order polynomial curve, and a/a_0 and b/b_0 vs. T are fitted linearly. Uncertainties of temperatures and unit-cell parameters are not presented because they are smaller than the sizes of the symbols.

cients α_0 are listed in Table 8. There are three different $\alpha_0(V)$ values for the entire temperature range and low- and high-temperature ranges. Values of $\alpha_0(V)$ for aragonite, strontianite, and witherite are essentially the same, considering the uncertainties, but much larger for cerussite. The $\alpha_0(V)$ of cerussite is about 20% larger than those of the other three carbonates for the entire temperature range, 10% larger for low-temperature range, and 30% larger over the high-temperature range. For each carbonate, $\alpha_0(c)$ is much greater than $\alpha_0(a)$ and $\alpha_0(b)$, indicating the carbonates have their largest thermal expansion coefficients in **c** direction, which is perpendicular to the plane of the CO_3 groups. The $\alpha_0(a)$ values are not significantly different, while $\alpha_0(b)$ values decrease in the order of aragonite > strontianite > witherite, and $\alpha_0(b)$ for cerussite is nearly the same as that for witherite. Then $\alpha_0(b)$ is larger than $\alpha_0(a)$ for aragonite, equal to $\alpha_0(a)$ for strontianite, and smaller than $\alpha_0(a)$ for cerussite and witherite (Figs. 2a–2d). The $\alpha_0(c)$ values increase in the order of aragonite < strontianite < witherite, "compensating" for the systematic decrease in $\alpha_0(b)$ values, so that $\alpha_0(V)$ remains nearly the same. The $\alpha_0(c)$ for cerussite is much larger, which accounts for the larger $\alpha_0(V)$ for cerussite relative to aragonite, strontianite, and witherite. In addition, as shown in Figure 2, c/c_0 values for cerussite vary more rapidly with temperature compared with those of the other carbonates.

Antao and Hassan (2010) report the axial and volumetric thermal expansion coefficients for aragonite as: $\alpha_0(a) = 9.8(1) \times 10^{-6}$ K^{-1}, $\alpha_0(b) = 21.2(3) \times 10^{-6}$ K^{-1}, $\alpha_0(c) = 39.8(5) \times 10^{-6}$ K^{-1}, and $\alpha_0(V) = 71(1) \times 10^{-6}$ K^{-1} for the temperature range of 298–750 K, and aragonite transformed to calcite ($R\bar{3}$c) above 750 K. The $\alpha_0(V)$ value is about 9% larger than our value (143–586 K). In addition, Antao and Hassan (2010) obtained $a_0 = 0.547(4) \times 10^{-4}$ K^{-1} and $a_1 = 6.1(2) \times 10^{-8}$ K^{-1} for aragonite $\alpha(V)$ of the same temperature range, which are 13 and 19% larger than our values, respectively. For witherite, Antao

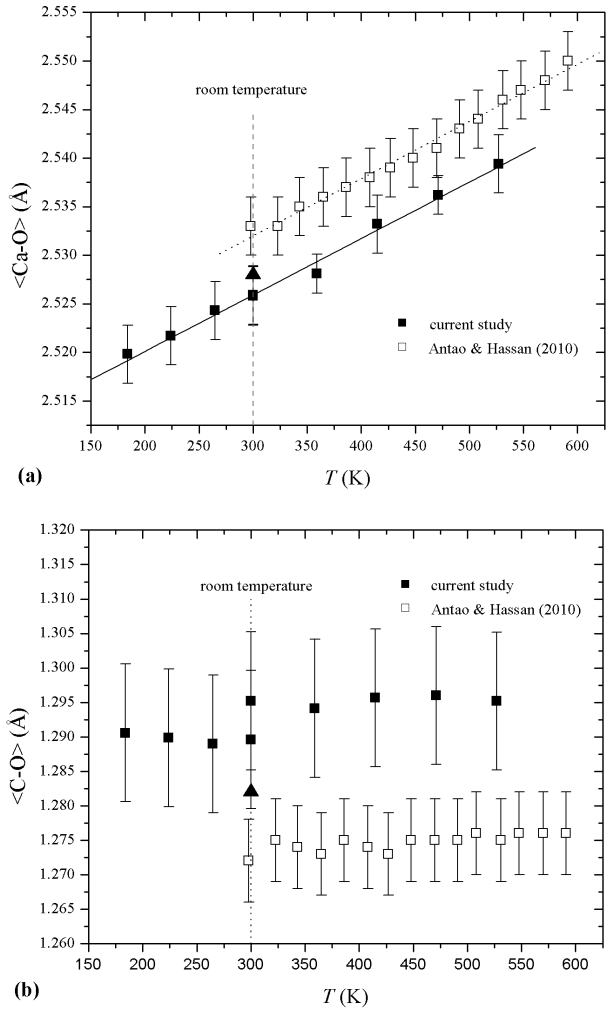

FIGURE 3. Average (**a**) <Ca-O> and (**b**) <C-O> bond lengths vs. *T* (K) for aragonite. <Ca-O> bond lengths vs. *T* are fitted linearly for both current study and Antao and Hassan (2010). The vertical error bars are for the uncertainties of bond lengths. The solid triangle symbols in **a** and **b** represent average bond lengths of aragonite from neutron diffraction (Jarosch and Heger 1986; Pokroy et al. 2007).

TABLE 7. The values of a_1, a_0, and *C* derived from the second-order polynomial fits to V/V_0

	a_1 (10^{-8} K^{-2})	a_0 (10^{-4} K^{-1})	*C*	R^2	T_{range} (K)
Aragonite	5.4(4)	0.46(2)	0.9837(4)	0.9998	143–586
Strontiante	3.6(7)	0.55(2)	0.9822(8)	0.9988	143–586
Cerussite	16.8(6)	0.27(3)	0.9842(5)	0.9998	143–489
Witherite	7.0(5)	0.39(3)	0.9847(5)	0.9996	143–586

TABLE 8. Average axial and bulk thermal expansion coefficients α_0 (10^{-6} K^{-1})

	$\alpha_0(a)$	$\alpha_0(b)$	$\alpha_0(c)$	$\alpha_0(V)$	$\alpha_0(V)$_low*	$\alpha_0(V)$_high†
Aragonite	9.1(6)	18.8(8)	37.1(6)	65(1)	58(2)	69(1)
Strontianite	12.7(5)	12.8(3)	43.1(9)	68(1)	58.3(7)	71(2)
Cerussite	11.0(2)	6.8(5)	62(2)	80(3)	64(2)	93(3)
Witherite	10.5(4)	6.0(2)	48(2)	65(2)	57(2)	70(2)

* For low-temperature range below 300 K.
† For high-temperature range above 300 K.

and Hassan (2007) reported: $\alpha_0(a) = 6.3(4) \times 10^{-6}$ K^{-1}, $\alpha_0(b) = 4.1(2) \times 10^{-6}$ K^{-1}, $\alpha_0(c) = 59.3(6) \times 10^{-6}$ K^{-1}, and $\alpha_0(V) = 69.5(4) \times 10^{-6}$ K^{-1} for the temperature range of 298–1067 K, and witherite transformed from space group of *Pmcn* to *R*3*m* above 1067 K. The $\alpha_0(V)$ value is about 7% larger than our value (143–586 K). For $\alpha(V)$ of witherite, $a_0 = 0.69(1) \times 10^{-4}$ K^{-1} and $a_1 = -0.3(3) \times 10^{-8}$ K^{-1}. No significant second-order thermal expansion was observed.

Liu et al. (2005) reported the linear axial compressibility of aragonite as: $\beta_0(a) = 3.0(2) \times 10^{-3}$ GPa^{-1}, $\beta_0(b) = 4.6(2) \times 10^{-3}$ GPa^{-1}, and $\beta_0(c) = 7.3(6) \times 10^{-3}$ GPa^{-1} by Brillouin spectroscopy; while Martinez et al. (1996) gave 2.4(2), 4.2(2), and 5.8(2) ($\times 10^{-3}$ GPa^{-1}) for $\beta_0(a)$, $\beta_0(b)$, and $\beta_0(c)$, respectively, for aragonite (up to 7.14 GPa at room temperature). Both studies give axial compressibilities in the order of $c > b > a$, which is in the same order as axial thermal expansion. Holl et al. (2000) reported that for witherite, $\beta_0(a) = 1.73(7) \times 10^{-3}$ GPa^{-1}, $\beta_0(b) = 1.49(1) \times 10^{-3}$ GPa^{-1}, and $\beta_0(c) = 16.8(3) \times 10^{-3}$ GPa^{-1} (to 7 GPa at room temperature), and at about 7.2 GPa, witherite transformed from *Pmcn* to $P\bar{3}1c$. The order of axial compressibilities for witherite is $c > a > b$, also consistent with the order of axial thermal expansion for witherite from the current study. In conclusion, the coherent orders of axial compressibility and thermal expansion support that aragonite group carbonates are most "flexible" in **c** direction, and aragonite is more "flexible" in **b** direction than in **a** direction, as opposed to witherite.

Crystal structure of aragonite at both low and high temperatures

After measurements of unit-cell parameters of aragonite, intensity scans were conducted for both low- and high-temperature ranges to investigate the changes of crystal structures with temperature. At ambient temperature, the <Ca-O> values from the point detector are 2.526(3) Å for both crystals of low- and high-temperature measurements, and <Ca-O> from CCD detector is 2.528(2) Å. <C-O> values at ambient temperature are 1.282(4), 1.29(1), and 1.30(1) Å for the intensity scans from CCD detector, point detector (after rigid-body correction) of low- and high-temperature measurements, respectively. All the three structure refinements yielded a <O-C-O> angle of 120.0(5)°. R_1 values for $I > 4\sigma$ remain systematically and coherently around ~2–3% for all refinements from point detector data at low- and high-temperatures. The bond lengths from CCD detector are more consistent with those from neutron diffractions (Jarosch and Heger 1986; Pokroy et al. 2007). For the intensity scans on point detector, the 2θ scans were limited to a smaller range, just in case that the heating prongs might block reflections of higher 2θ. The difference of ambient <C-O> values for the two crystals from point detector is smaller than the uncertainties of the measurements.

<Ca-O> and rigid-body corrected <C-O> vs. *T* (K) are plotted in Figures 3a and 3b, respectively, comparing with the values from Antao and Hassan (2010), as well as the ones from neutron diffractions at ambient temperature. The data from Antao and Hassan (2010) are plotted over part of their temperature range to 590 K, instead of the whole range up to 750 K. <Ca-O> at ambient temperature from current study is about 0.006 Å smaller than that from Antao and Hassan (2010).

The linear fittings for the two data sets are almost parallel to each other.

$$\text{Current study: } \langle Ca\text{-}O\rangle = 5.8(8) \times 10^{-6} \times T + 2.508(3) \quad (5)$$

$$\text{Antao and Hassan (2010): } \langle Ca\text{-}O\rangle = 5.9(8) \times 10^{-6} \times T + 2.514(4) \quad (6)$$

The discrepancies of <Ca-O> and <C-O> values between this study and Antao and Hassan (2010) could be attributed to different experimental apparatuses. The data of Antao and Hassan (2010) were derived from in situ synchrotron powder X-ray diffraction, with $\lambda = 0.61684(5)$ Å and $2\theta < 30°$. On the other hand, despite the differences among the samples, the three data sets of <C-O> for low- and high-temperature measurements of the current study and Antao and Hassan (2010) remain the same within errors over the temperature ranges studied, respectively, implying that CO_3 groups can be treated as rigid bodies during thermal expansion.

Acknowledgments

This work was supported by U.S. National Science Foundation grants EAR 07-11165 and 11-13369. The electron-microprobe analyses were conducted by John W. Drexler.

References cited

Antao, S.M. and Hassan, I. (2007) $BaCO_3$: High-temperature crystal structures and the *Pmcn* → *R*3*m* phase transition at 811 °C. Physics and Chemistry of Minerals, 34, 573–580.

——— (2009) The orthorhombic structure of $CaCO_3$, $SrCO_3$, $PbCO_3$ and $BaCO_3$: Linear structural trends. The Canadian Mineralogist, 47, 1245–1255.

——— (2010) Temperature dependence of the structural parameters in the transformation of aragonite to calcite, as determined from in situ synchrotron powder X-ray-diffraction data. The Canadian Mineralogist, 48, 1225–1236.

Baker, E.H. (1962) A high-temperature form of strontium carbonate. Journal of the Chemistry Society (Resumed), p. 2525–2526.

Bevan, D.J.M., Rossmanith, E., Mylrea, D.K., Ness, S.E., Taylor, M.R., and Cuff, C. (2002) On the structure of aragonite—Lawrence Bragg revisited. Acta Crystallographica, B58, 448–456.

Bragg, W.L. (1924) The structure of aragonite. Proceedings of The Royal Society London A, 105, 16–39.

Bruker (1996) XSCANS software package. Bruker AXS Incorporation, Madison, Wisconsin, U.S.A.

Caspi, E.N., Pokroy, B., Lee, P.L., Quintana, J.P., and Zolotoyabko, E. (2005) On the structure of aragonite. Acta Crystallographica, B61, 129–132.

Chevrier, G., Giester, G., Heger, G., Jarosch, D., Wildner, M., and Zemann, J. (1992) Neutron single-crystal refinement of cerussite, $PbCO_3$, and comparison with other aragonite-type carbonates. Zeitschrift für Kristallographie, 199, 67–74.

Dal Negro, A. and Ungaretti, L. (1971) Refinement of the crystal structure of aragonite. American Mineralogist, 56, 768–772.

De Villiers, J.P.R. (1971) Crystal structures of aragonite, strontianite, and witherite. American Mineralogist, 56, 758–767.

Dickens, B. and Bowen, J.S. (1971) Refinement of the crystal structure of the aragonite phase of $CaCO_3$. Journal of Research of the National Bureau of Standards, A, 75, 27–32.

Downs, R.T., Bartelmehs, K.L., Gibbs, G.V., and Boisen, M.B. Jr. (1992) Variations of bond lengths and volumes of silicate tetrahedral with temperature. American Mineralogist, 77, 751–757.

——— (1993) Interactive software for calculating and displaying X-ray or neutron powder diffractometer patterns of crystalline materials. American Mineralogist, 78, 1104–1107.

Farrugia, L.J. (1999) WinGX software package. Journal of Applied Crystallography, 32, 837–838.

Hazen, R.M., Downs, R.T., and Prewitt, C.T. (2000) Principles of comparative crystal chemistry. In R.M. Hazen and R.T. Downs, Eds., High-Temperature and High-Pressure Crystal Chemistry, 41, p. 1–34. Reviews in Mineralogy and Geochemistry, Mineralogical Society of America, Chantilly, Virginia.

Holl, C.M., Smyth, J.R., Laustsen, H.M.S., Jacobsen, S.D., and Downs, R.T. (2000) Compression of witherite to 8 GPa and the crystal structure of $BaCO_3$ II. Physics and Chemistry of Minerals, 27, 467–473.

Jarosch, D. and Heger, G. (1986) Neutron diffraction refinement of the crystal structure of aragonite. Tschermaks Mineralogische und Petrographische Mitteilungen, 35, 127–131.

——— (1988) Neutron diffraction investigation of strontianite, $SrCO_3$. Bulletin de Minéralogie, 111, 139–142.

Lander, J.J. (1949) Polymorphism and anion rotational disorder in the alkaline earth carbonates. The Journal of Chemical Physics, 17, 892–901.

Lin, C.-C. and Liu, L.-G. (1996) Post-aragonite phase transitions in strontianite and cerussite—A high-pressure Raman spectroscopic study. Journal of Physics and Chemistry of Solids, 58, 977–987.

——— (1997) High pressure phase transformations in aragonite-type carbonates. Physics and Chemistry of Minerals, 24, 149–157.

Liu, L.-G., Chen, C.-C., Lin, C.-C., and Yang, Y.-J. (2005) Elasticity of single-crystal aragonite by Brillouin spectroscopy. Physics and Chemistry of Minerals, 32, 97–102.

Martinez, I., Zhang, J., and Reeder, R.J. (1996) In situ X-ray diffraction of aragonite and dolomite at high pressure and high temperature: Evidence for dolomite breakdown to aragonite and magnesite. American Mineralogist, 81, 611–624.

Pannhorst, W. and Löhn, J. (1970) Zur kristallstruktur von strontianit, $SrCO_3$. Zeitschrift für Kristallographie, 131, 455–459.

Pilati, T., Demartin, F., and Gramaccioli, C.M. (1998) Lattice-dynamical estimation of atomic displacement parameters in carbonates: calcite and aragonite $CaCO_3$, dolomite $CaMg(CO_3)_2$, and magnesite $MgCO_3$. Acta Crystallographica, B54, 515–523.

Pokroy, B., Fieramosca, J.S., Von Dreele, R.B., Fitch, A.N., Caspi, E.N., and Zolotoyabko, E. (2007) Atomic structure of biogenic aragonite. Chemistry of Materials, 19, 3244–3251.

Sheldrick, G.M. (1997) SHELXL97, Release 97-2. Program from the refinement of crystal structures. University of Göttingen, Germany.

Speer, J.A. (1983) Crystal chemistry and phase relations of the orthorhombic carbonates, In R.J. Reeder, Ed., Carbonates, 11, p. 145–190. Reviews in Mineralogy and Geochemistry, Mineralogical Society of America, Chantilly, Virginia.

Weinbruch, S., Büttner, H., and Rosenhauer, M. (1992) The orthorhombic-hexagonal phase transformation in the system $BaCO_3$-$SrCO_3$ to pressures of 7000 bar. Physics and Chemistry of Minerals, 19, 287–297.

Wyckoff, R.W.G. (1925) Orthorhombic space group criteria and their applications to aragonite. American Journal of Science, 209, 145–175.

Ye, Y., Schwering, R.A., and Smyth, J.R. (2009) Effects of hydration on thermal expansion of forsterite, wadsleyite, and ringwoodite at ambient pressure. American Mineralogist, 94, 899–904.

Manuscript received June 25, 2011
Manuscript accepted December 8, 2011
Manuscript handled by Hongwu Xu